Since January 2020 Elsevier has created a COVID-19 resource centre with free information in English and Mandarin on the novel coronavirus COVID-19. The COVID-19 resource centre is hosted on Elsevier Connect, the company's public news and information website.

Colloids and Surfaces B: Biointerfaces 102 (2013) 265–272

Contents lists available at SciVerse ScienceDirect

Colloids and Surfaces B: Biointerfaces

journal homepage: www.elsevier.com/locate/colsurfb

Synthesis of Fe_3O_4@silica/poly(*N*-isopropylacrylamide) as a novel thermo-responsive system for controlled release of $H_3PMo_{12}O_{40}$ nano drug in AC magnetic field

Javidi Jaber [a,*], Esmaeilpour Mohsen [b]

[a] Institute of Nano Science and Nano Technology, University of Kashan, Kashan, Iran
[b] Chemistry Department, College of Science, Shiraz University, Shiraz 71454, Iran

ARTICLE INFO

Article history:
Received 29 May 2012
Received in revised form 14 August 2012
Accepted 16 August 2012
Available online 24 August 2012

Keywords:
Heteropolyacids
Thermo-responsive
Controlled release
Magnetic field
Nano-drug

ABSTRACT

In this work, a new method is introduced for synthesis of nano drug for the first time. $H_3PMo_{12}O_{40}$ and Fe_3O_4@SiO_2/poly(*N*-isopropylacrylamide), were prepared as nano drug and magneto thermally responsive nano-carrier respectively. Then the released behavior of $H_3PMo_{12}O_{40}$ nano-drug from this thermo-responsive carrier was investigated in an AC magnetic field. When a drug particle is broken up to nanometer range, the total surface area is increased; therefore the rate of dissolution and the rate of release are increased. The as-synthesized nanostructures were characterized by scanning electron microscopy (SEM), X-ray powder diffraction (XRD), transmission electron microscopy (TEM), vibrating sample magnetometer (VSM), and Fourier transform infrared spectroscopy (FT-IR). Furthermore, experimental condition which lead to the released profile of $H_3PMo_{12}O_{40}$ nano-drug from Fe_3O_4@SiO_2/poly(*N*-isopropylacrylamide), such as strength of magnetic field (H), temperature (T), particle size of drug and content of loaded drug were tested. Increasing the strength of magnetic field, temperature and content of loaded drug, the rate of drug release was also increased.

1. Introduction

Heteropolyacids (HPAs) as classes of inorganic compound are transition metal oxide clusters that contain W, Mo and V metals. These materials have an impressive application potential in optics, electronics, catalysis and medicines [1–3]. Rhule et al. published a review and described the applications of HPAs in medicines [4]. HPAs have been shown to exhibit antiviral activity against several RNA viruses including the orthomyxoviruses, paramyxoviruses, flaviviruses, coronaviruses, retroviruses, different influenza strains, Dengue fever virus and SARS coronavirus [5–7]. Also, HPAs have been investigated as promising anti-HIV [8] and anti-cancer agents [9,10]. The activity of HPAs is dependent on their particle size. A novel method for synthesis of HPAs with nanometer size was introduced in this work for the first time.

Magnetothermally-triggered drug delivery systems offer a novel mechanism by which release of a drug can be triggered externally to the body [11]. When magnetic materials are exposed to a magnetic field of strength H, the magnetic induction (B) in these materials is represented by Eq. (1):

$$B = \mu_0(H + M) \tag{1}$$

Here, μ_0 is the permeability in vacuum and M is the magnetic moment per volume. When these materials are placed in an AC magnetic field, power dissipation of these particles from heat caused by the delay in the relaxation of the magnetic moment through either the rotation within the particle (Néel relaxation (τ_N)) or the rotation of the particle itself (Brownian relaxation (τ_B)) [12]. The effective relaxation time τ is given by Eq. (2):

$$\frac{1}{\tau} = \frac{1}{\tau_B} + \frac{1}{\tau_N} \tag{2}$$

The power dissipation is expressed as [13]:

$$P = \pi\mu_0\chi_0 H^2 f \frac{2\pi f\tau}{1 + (2\pi f\tau)^2} \tag{3}$$

where, χ_0 is the actual volumetric magnetic susceptibility, f is the frequency of the applied AC magnetic field. Temperature rise for these magnetic materials is related to power dissipation and computed by Eq. (4):

$$\Delta T = P\frac{\Delta t}{C} \tag{4}$$

* Corresponding author. Tel.: +98 7116137738; fax: +98 7112286008.
E-mail address: Jaberjavidi@gmail.com (J. Jaber).

0927-7765/$ – see front matter © 2012 Elsevier B.V. All rights reserved.
http://dx.doi.org/10.1016/j.colsurfb.2012.08.024

Here, C is the fluid specific heat and Δt is the duration of the heating. As shown in Eqs. (3) and (4) the temperature rise is dependent on the strength of the AC magnetic field. In most cases, higher field intensities generate more heat [14]. But in the definite temperature, the magnetic material will stop heating and reach steady state, even if the AC magnetic field is applied for a long period of time. This temperature, known as Curie temperature, which is dependent on the crystal size as nanomagnetic materials has low Curie temperature [11,14].

Thermo-sensitive polymers have been extensively studied for controlled release drug delivery. These polymers are including poly(*N*-isopropylacrylamide) (PNIPAM) [15–17], poly(vinyl methyl ether) (PVME) [18], and poly(ethylene oxide)-poly(propylene oxide)-poly(ethylene oxide) (PEOePPOePEO) tri-block copolymers [19]. These polymers have a distinctive lower critical solution temperature (LCST) and are water insoluble at temperatures above their LCSTs. In water, PNIPAM hydrogels show a negative volume response to temperature, due to a phase transition occurs in the polymer configuration: they maintain a swollen (hydrophilic) state at low temperature, while they shrink remarkably to a collapsed (hydrophobic) state when the temperature is raised above 32 °C, which is PNIPAM's lower critical solution temperature [20]. Due to the dramatic volume phase transition properties, PNIPAM-based hydrogel has been used in the thermo-responsive controlled release [21–26], protein adsorption and heavy metal ion adsorbent, cell detachment and so on [27–30].

Recently, a number of functionalized Fe_3O_4 nanoparticles have been employed and the studies on immobiliztation of catalysts on silica coated ironoxide nanoparticles have been reported [31–33]. Also, in recent years, Fe_3O_4@C@PANI magnetic microspheres for the extraction and analysis of phenolic compounds and core–shell microspheres with PNIPAM core and biocompatible porous ethyl cellulose shell embedded with PNIPAM gates have been successfully prepared [34,35].

In this work, we prepared $H_3PMo_{12}O_{40}$ nano-drug as HPAs agents and Fe_3O_4@SiO_2/poly(*N*-isopropylacrylamide) as magnetothermally responsive carrier for the first time. Then the released behavior of $H_3PMo_{12}O_{40}$ nano-drug from this thermo-responsive carrier in an AC magnetic field was investigated.

Furthermore, experimental condition such as strength of magnetic field (H), temperature (T), particle size and content of loaded drug which lead to the released profile of $H_3PMo_{12}O_{40}$ nano-drug from Fe_3O_4@SiO_2/poly(*N*-isopropylacrylamide), were tested.

2. Experimental

2.1. Materials and physical measurements

All the chemical reagents used in our experiments were of analytical grade and were used as received without further purification. X-ray powder diffraction (XRD) patterns were recorded by a Rigaku D-max C III, X-ray diffractometer using Nifiltered Cu Kα radiation. Dynamic light scatterings (DLS) were recorded on a HORIBA-LB550. Scanning electron microscopy (SEM) image was obtained on Philips XL-30ESEM. Transmission electron microscopy (TEM) images were obtained on a Philips EM208 transmission electron microscope with an accelerating voltage of 100 kV. Fourier transform infrared (FT-IR) spectra were recorded on Shimadzu Varian 4300 spectrophotometer in KBr pellets. Magnetic properties were obtained on a BHV-55 vibrating sample magnetometer (VSM).

2.2. Synthesis of $H_3PMo_{12}O_{40}$ nano drug

$H_3PMo_{12}O_{40}$ nanoparticles (which were labeled as PMA^n) were prepared using the solvothermal method in an n-Octane as salvent. In a typical procedure, 5 mmol of bulk $H_3PMo_{12}O_{40}$ (PMA^b) was dispersed in 50 ml n-Octane and the resulting dispersion was stirred vigorously for 30 min at room temperature to form a homogeneous dispersion. This solution was transferred into a Teflon-lined stainless autoclave filling 80% of the total volume. The autoclave was sealed and maintained at 150 °C for 12 h. The autoclave was then cooled to room temperature. Finally, the resulted powder was filtered and washed for several times by n-Octane, and dried in a vacuum at 80 °C for 12 h.

2.3. Synthesis of Fe_3O_4@ silica mesoporous

For synthesis of Fe_3O_4@ silica mesoporous, Fe_3O_4 nanoparticles were prepared first. In a typical procedure the mixture of $FeCl_3{\cdot}6H_2O$ (1.3 g, 4.8 mmol) in water (15 ml) was added to the solution of CTAB (1 g), as a surfactant, and $FeCl_2{\cdot}4H_2O$ (0.9 g, 4.5 mmol) in water (15 ml), which was prepared by completely dissolving CTAB in water followed by addition of $FeCl_2{\cdot}4H_2O$. The resultant solution was left to be stirred for 30 min in 80 °C. Then ethylenediamine (1.0 mol/l) was added drop by drop with vigorous stirring to produce a black solid product when the reaction media reaches pH 10. The resultant mixture was heated on water bath for 2 h at 60 °C and the black magnetite solid product was filtered and washed with ethanol three times and was then dried at 80 °C for 10 h.

The core–shell Fe_3O_4@SiO_2/CTAB nanospheres were prepared by a modified Stober method [36]. Briefly, Fe_3O_4 (0.50 g, 2.1 mmol) was dispersed in the mixture of ethanol (50 ml), deionized water (5 ml), CTAB (0.5 g) and tetraethoxysilane (TEOS) (0.20 ml), after that 5.0 ml of NaOH (10 wt%) was added. This solution was stirred mechanically for 30 min at room temperature. Then the product, Fe_3O_4@SiO_2/CTAB, was separated by an external magnet, and was washed with deionized water and ethanol three times and dried at 80 °C. For preparing Fe_3O_4@ silica mesoporous, the as-synthesis Fe_3O_4@SiO_2/CTAB was calcined at 600 °C.

2.4. Synthesis of Fe_3O_4@silica/PIPA

For synthesis of Fe_3O_4@silica/PIPA, first of all *N*-isopropylacrylamide (72 mmol), *N*,*N*′-methylene-bis(acrylamide) (2 mmol) and benzoeil peroxide (2 mmol) were mixed with 50 ml acetone and were placed under a stream of nitrogen. Then 5 g of Fe_3O_4@SiO_2 synthesis was added to above solution and this solution was heated for 18 h at 60 °C. The resulting gel was filtered and washed three times with acetone. Then, for removal of unloaded PIPA from Fe_3O_4@SiO_2 and in order to excess *N*-isopropylacrylamide, *N*,*N*′-methylene-bis(acrylamide) or benzoeil peroxide, the resulting gel was redispersed in 50 ml acetone and extracted with external magnetic field [26].

2.5. Loaded of PMA^n in Fe_3O_4@silica/PIPA

For loading PMA^n in Fe_3O_4@silica/PIPA, 1.0 g Fe_3O_4@silica loaded with PIPA gel was added to an aqueous PMA^n solution and stirred for 24 h at room temperature. This procedure was repeated by PMA^b. The loading capacity and the encapsulation efficiency of the silica nanoparticles were calculated according to the following formula:

$$\text{Drug loading capacity} = \frac{(W_{\text{administered dose}} - W_{\text{residual dose in solution}})}{W_{\text{nano-carrier}}}$$

Table 1
Experimental conditions of loading and releasing of PMA.

Sample	(mg)	Loaded PMA (mg)	T (°C)	t_0[a] (min)	H (G)	Released PMA after 10 h (mg)	Released PMA after 10 h (%)
1	50	30	45	15	520	25.0	83.3
2	70	40	45	15	520	36.0	90.0
3	90	70	45	15	520	64.0	91.4
4	110	80	45	15	520	75.0	93.8
5	90	70	35	15	500	57.5	82.1
6	90	70	40	15	510	60.0	85.7
7	90	70	50	20	550	65.0	92.8
8	90	70	55	20	570	67.5	96.4
9	PMA[b] (90 mg)	30	45	20	520	10	33.3

[a] Time required for constant temperature.

$$\text{Encapsulation efficiency} = \frac{(W_{\text{administered dose}} - W_{\text{residual dose in solution}})}{W_{\text{administered dose}}} \times 100\%$$

where $W_{\text{administered dose}}$ is the weight of PMA^n or PMA^b as drug for loading, $W_{\text{residual dose in solution}}$ is the weight of residual PMA^n or PMA^b in solution after loading onto Fe_3O_4@silica/PIPA nanoparticle, and $W_{\text{nano-carrier}}$ is the weight of Fe_3O_4@silica/PIPA nanoparticles for loading, respectively.

2.6. In vitro release of PMA from Fe_3O_4@silica/PIPA

In vitro release of PMA was performed by immersing 0.1 g PMA-encapsulated Fe_3O_4@silica/PIPA in 50 ml simulated body fluid (SBF) at 37 °C. The SBF was prepared by dissolving reagent grade NaCl, $NaHCO_3$, KCl, $Na_2HPO_4{\cdot}2H_2O$, $MgCl_2{\cdot}6H_2O$, $CaCl_2{\cdot}2H_2O$, and Na_2SO_4 in deionized water. The solution was buffered to pH 7.4 with Tris buffer and hydrochloric acid. This solution is exposed to an AC magnetic field with 350 kHz frequency. Then at predetermined time intervals, 5 ml of the solution was collected from the released medium and replaced with fresh SBF. The released PMA was analyzed by UV/vis spectrophotometer. By changing the intensity of the magnetic field, the temperature of released medium was controlled. Table 1 shows the conditions of loading and releasing of PMA in detail. Also, experimental procedure and experimental setup are shown in Fig. 1a and b respectively.

The heat generation of Fe_3O_4@silica nano-carriers that were dispersed in simulated body fluid was investigated by a custom-designed magnetic-induction chamber. The concentration of Fe_3O_4@silica nanoparticles aqueous suspension was adjusted to

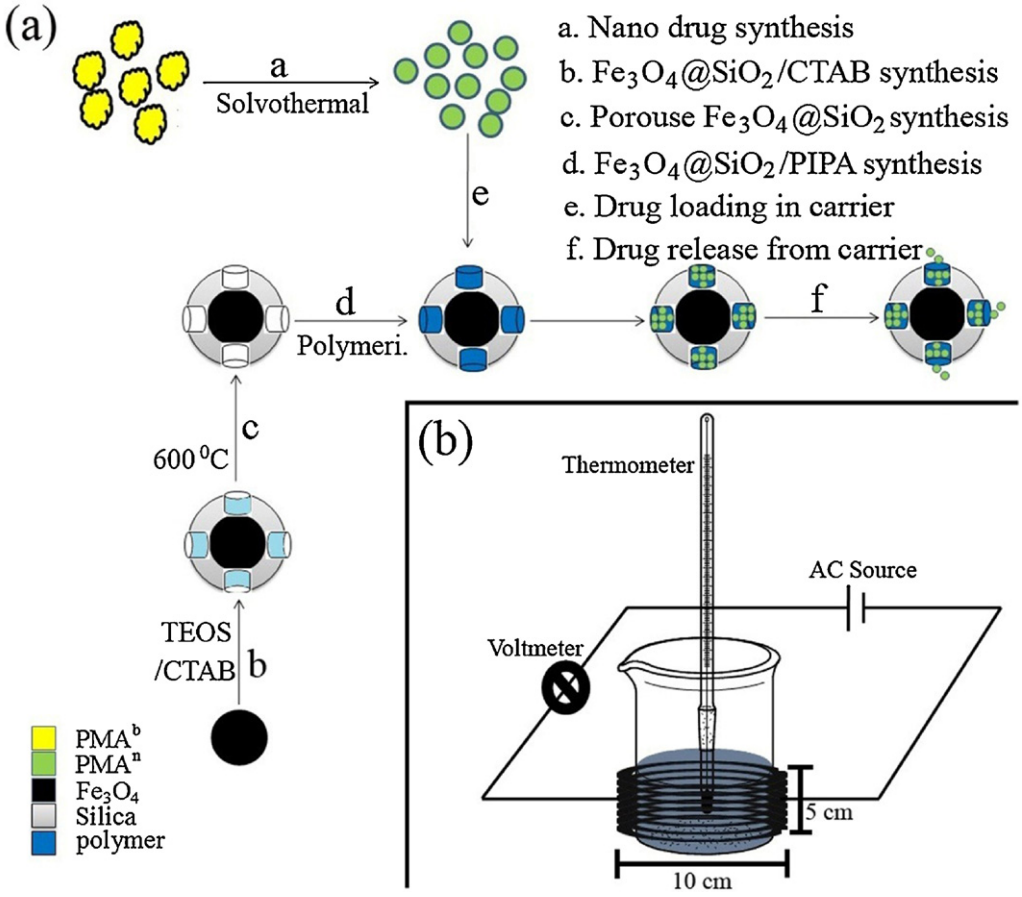

Fig. 1. Experimental procedure (a) and experimental setup (b).

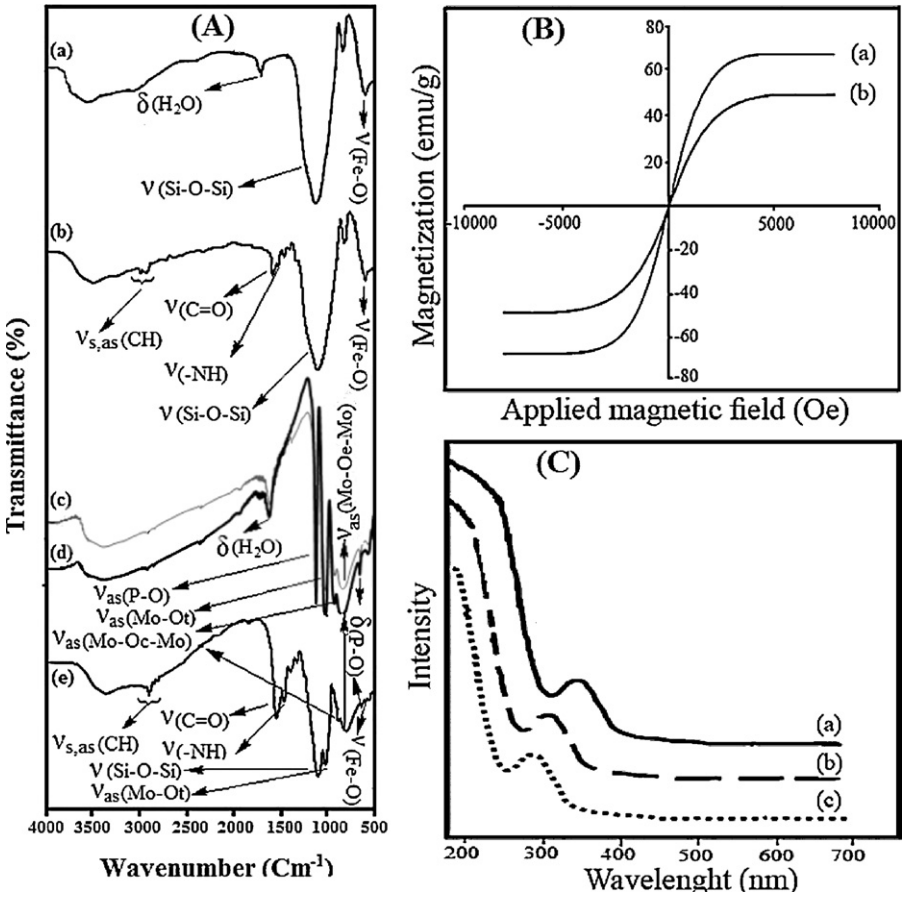

Fig. 2. (A) The FT-IR spectra of (a) Fe_3O_4@SiO_2, (b) Fe_3O_4@silica/PIPA, (c) $H_3PMo_{12}O_{40}$ nanoparticle (PMA^n), (d) $H_3PMo_{12}O_{40}$ bulk (PMA^b) and (e) synthesized Fe_3O_4 @ SiO_2/PIPA/PMA^n sample, (B) magnetization curves at 300 K for Fe_3O_4 (a) and Fe_3O_4@silica/PIPA/PMA^n (b) and (C) UV spectra of PMA^b (a), PMA^n (b) and Fe_3O_4@silica/PIPA/PMA^n (c). (For interpretation of the references to color in this figure legend, the reader is referred to the web version of the article.)

10 mg/ml. The heating setup is composed of a power supply (Nova Star 5 kW RF Power Supply, Ameritherm, Inc., Scottsville, NY, USA), coil (Induction Atmospheres, Rochester, NY, USA) and chiller (JT1000; Refrigerant: R-134A, pressure: 200 psi, Koolant Koolers INC., Kalamazoo, MI, USA). The magnetic field was controlled by adjusting the voltages in the power supply. The rising temperatures were measured using digital thermometer every 30 s for 20 min. The temperature of the Fe_3O_4@silica nano-carriers suspension (50 ml) under various AC magnetic fields was measured in the center of samples through the gaps in the coils by thermometer. These data were used to generate heating profiles for each sample. The dependence on the applied AC magnetic field of heat generation was investigated at frequencies of 350 kHz with magnetic fields ranging from 500 to 570 G.

3. Results and discussion

The elemental analysis of PMA^n nanoparticles was estimated by ICPAES. The Mo/P ratio of the PMA^n was 12.4. Therefore these nanoparticles have Keggin unit cell structure because Keggin units

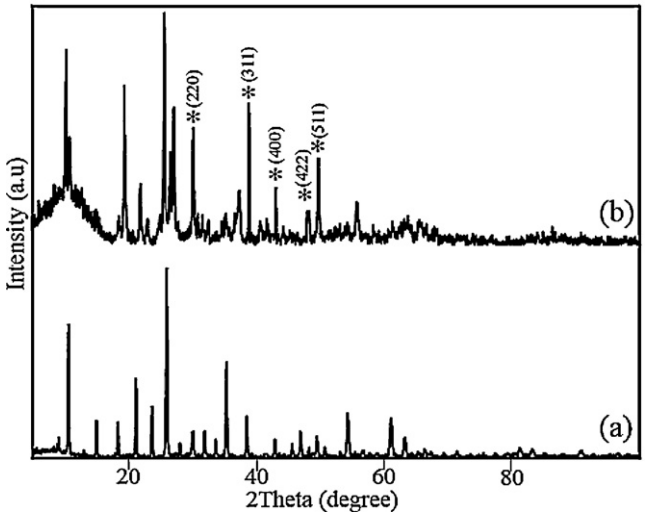

Fig. 3. XRD patterns of PMA^n (a) and Fe_3O_4@silica/PIPA/PMA^n (b).

Table 2
The characteristic bands of PMA^n and Fe_3O_4@silica/PIPA/PMA^n.

Sample	PMA^n				Fe_3O_4@silica/PIPA/PMA^n				
	O^*	O_c	O_e	O_t	Fe—O	Si—O—Si	C—H	C=O	N—H
Wavenumber (cm^{-1})	1063	839	755	955	563	1000–1150	2850–3000	1653	1544

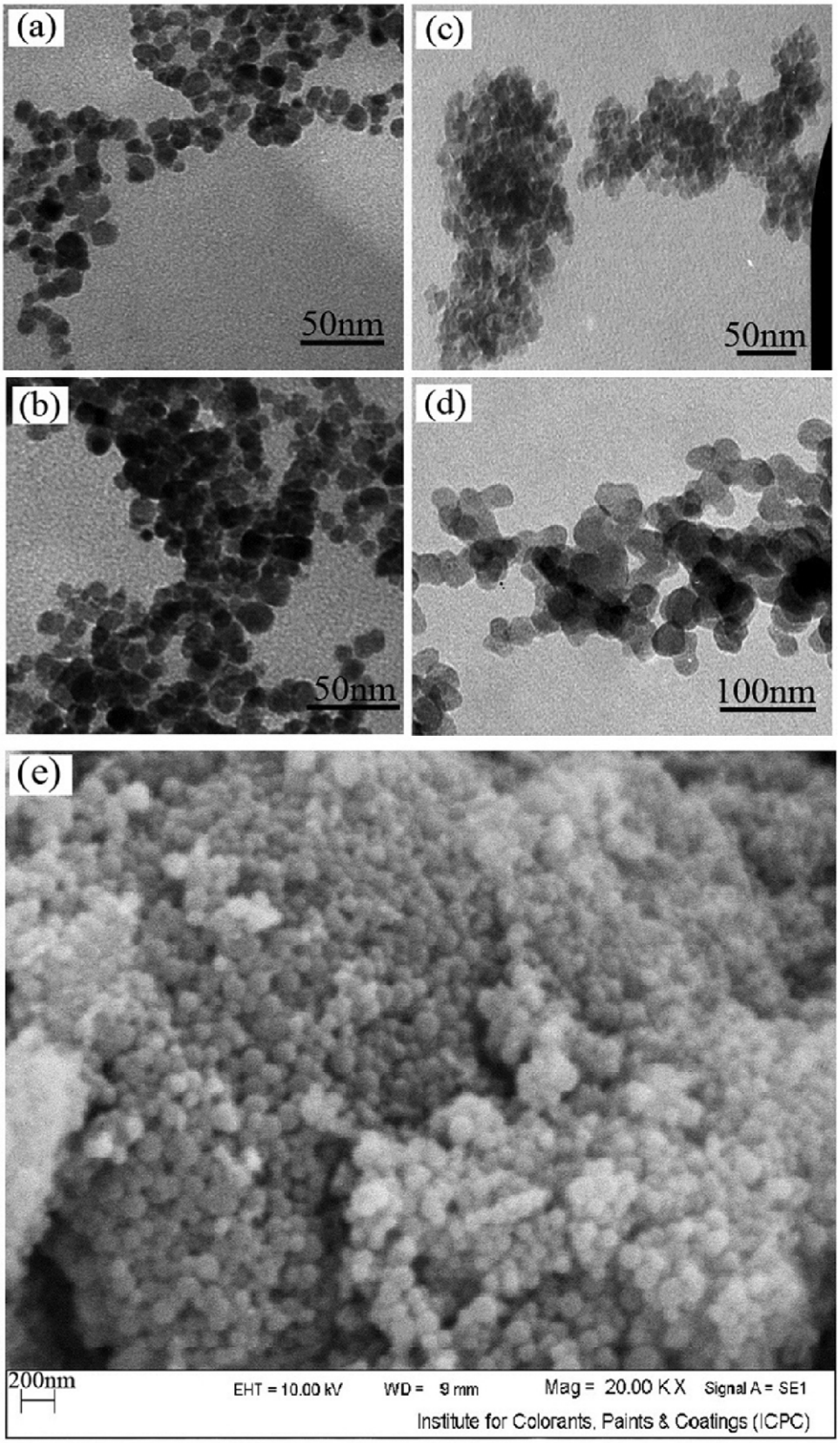

Fig. 4. TEM images of Fe_3O_4 (a), PMA^n (b), Fe_3O_4@silica (c) and Fe_3O_4@silica/PIPA/PMA^n (d) respectively and SEM image of Fe_3O_4@silica/PIPA/PMA^n (e).

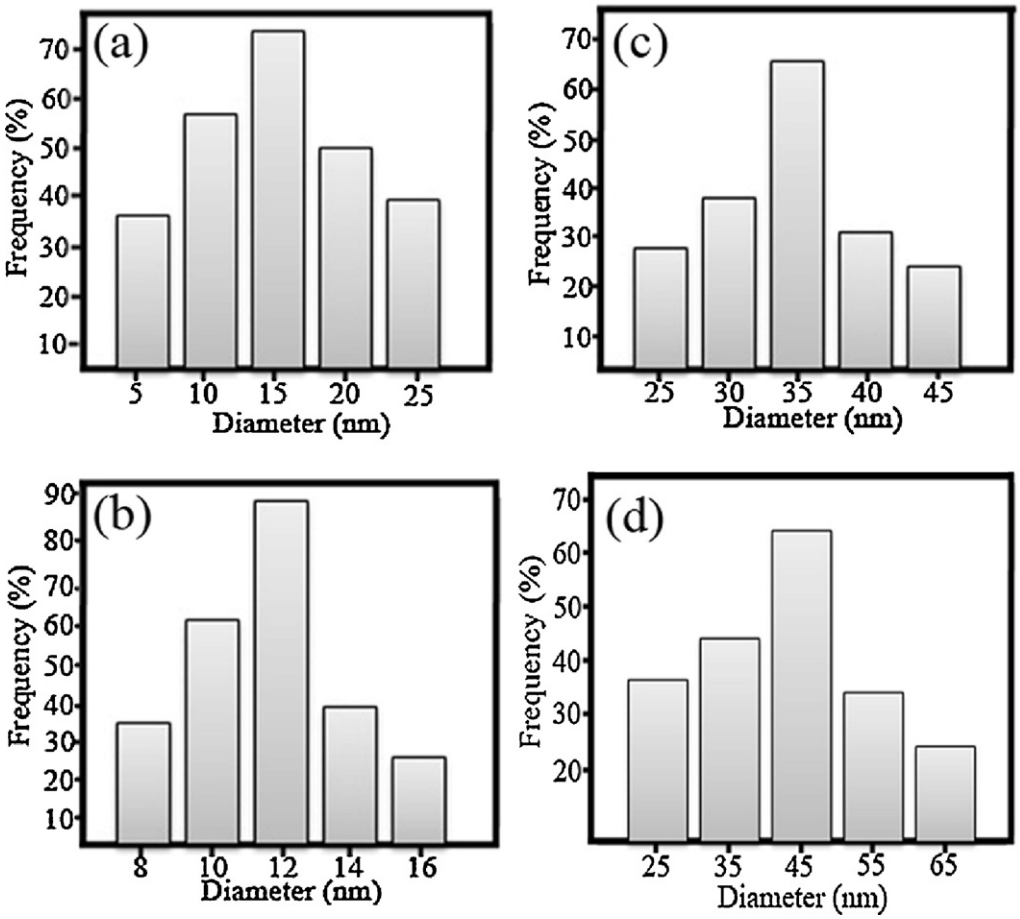

Fig. 5. Particle size histograms of Fe_3O_4 (a), PMA^n (b), Fe_3O_4@silica (c) and Fe_3O_4@silica/PIPA/PMA^n (d) respectively.

have one central atom (P), 12 transition metal atoms (Mo) and an appropriate number of charge balancing protons or cations.

PMA with Keggin structure consisted of one PO_4 tetrahedron surrounded by four Mo_3O_{13} sets formed by three edge-sharing octahedra. There are four types of oxygen atoms in $H_3PMo_{12}O_{40}$; O^* (the central oxygen atoms in PO_4 tetrahedron), O_c (the corner-sharing oxygen between different Mo_3O_{13} sets), O_e (the edge-sharing oxygen-bridge within Mo_3O_{13} sets), and O_t (the terminal oxygen atoms) [37].

Fig. 2A shows the FT-IR spectra of (a) Fe_3O_4@SiO_2, (b) Fe_3O_4@silica/PIPA, (c) $H_3PMo_{12}O_{40}$ nanoparticle (PMA^n), (d) $H_3PMo_{12}O_{40}$ bulk (PMA^b) and (e) synthesized Fe_3O_4@SiO_2/PIPA/PMA^n sample. Fe_3O_4@SiO_2 shows vibration bands in 561, 1000–1150, and 3400 cm^{-1}, which can be attributed to the Fe—O, Si—O—Si, and —OH bonds, respectively (Fig. 2Aa). Fig. 2Ab shows the FT-IR spectrum of Fe_3O_4@silica/PIPA nanoparticles, the peaks at 562, 1000–1150, 1546 and 1655 cm^{-1} are attributed to Fe—O (stretching vibration), Si—O—Si (asymmetric stretching), N—H (bending) and C=O (stretching), respectively. The presence of several bands with medium intensity in 2850–2980 cm^{-1} region is allocated to C—H stretching of groups (symmetric and asymmetric stretching). These results indicated that poly (*N*-isopropylacrylamide) was coated on the Fe_3O_4@SiO_2 successfully. The FT-IR spectrum for PMA^n shows four bands corresponding to the Keggin structure at 755, 839, 955 and 1063 cm^{-1}, which can be assigned to ν_{as}(Mo–O_e–Mo), ν_{as}(Mo–O_c–Mo), ν_{as}(Mo–O_t) and ν_{as}(P–O^*), respectively (Fig. 2Ac). It also shows a weak band in the region of 590 cm^{-1} which corresponds to the δ(P–O) vibration. According to FT-IR spectroscopy, the characteristic bands for PMA^n compared to PMA^b, are shifted to higher wave numbers (blue shift). The binding of PMA^n on surfaces of Fe_3O_4@silica/PIPA magnetic nanoparticles was confirmed by FTIR spectroscopy (Fig. 2Ae). The absorption bands at 563, 1000–1150, 1544, 1653 and 2850–3000 cm^{-1} are in correspondence with vibrations of Fe—O, Si—O—Si, N—H, C=O and C—H stretching in Fe_3O_4@silica/PIPA nanoparticles [38–41] and also, the appearance of the peaks at 756, 840, 955 and 1065 cm^{-1} that are in correspondence with PMA^n, confirmed that PMA^n was coated on the Fe_3O_4@silica/PIPA magnetic nanoparticles successfully. The characteristic bands for these samples are listed in Table 2.

The magnetic properties of the samples were studied by a vibrating sample magnetometer at 300 K. Fig. 2Ba and b show the magnetic hysteresis loops of Fe_3O_4 and Fe_3O_4@silica/PIPA/PMA^n respectively. As it is shown, the hysteresis phenomenon was not found and the magnetization and demagnetization curves were coincident. This indicated that all products had super-para magnetism at room temperature. The saturation magnetization values for Fe_3O_4 and Fe_3O_4@silica/PIPA/PMA^n were 65.0 and 46.0 emu/g, respectively

X-ray powder diffraction patterns of PMA^n and Fe_3O_4@silica/PIPA/PMA^n are shown in Fig. 3a and b respectively. The strong characteristic peaks at $2\theta = 9.05^\circ$, 23.7°, 26.35°, 28.25° and 32.4° in Fig. 3a, are assigned to Keggin structure of PMA [JCPDS File 1-32] [42]. No other peak exists in this pattern, showing the high purity and well crystallinity of the samples.

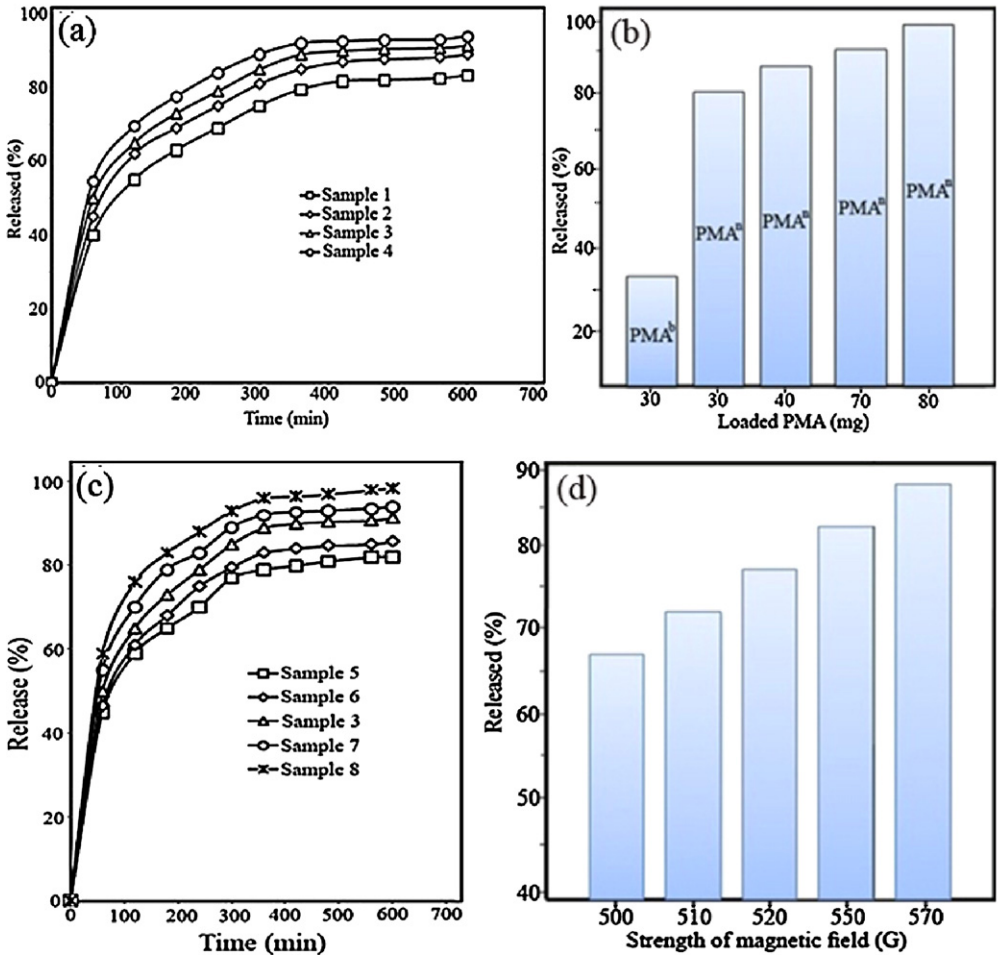

Fig. 6. The release profiles of PMA from Fe_3O_4@silica/PIPA/PMA in different loaded PMA (a and b). The release profiles of PMA from Fe_3O_4@silica/PIPA/PMA in different (c) temperature and (d) strength of magnetic field.

The characteristic peaks in Fig. 3b, which were indicated by star (*) corresponded with cubic Fe_3O_4 (JCPDS# 19-629) [43]. From XRD data, the crystallite size (D_c) of the as-prepared PMA^n, were calculated using the Debey–Scherrer equation [44],

$$D_c = \frac{K\lambda}{\beta \cos\theta}$$

where, β is the breadth of the observed diffraction line at its half-intensity maximum, k is the so-called shape factor, which usually takes a value of about 0.9, and k is the wavelength of X-ray source used in XRD. The average size of the PMA^n, were calculated to be 18 nm, which is to some extent in agreement with the one observed from TEM and DLS images.

TEM and DLS images of the nanoparticels have been represented in Figs. 4 and 5. Fig. 4a–d shows TEM images of Fe_3O_4, PMA^n, Fe_3O_4@silica and Fe_3O_4@silica/PIPA/PMA^n respectively. The size of nanoparticles obtained from the TEM images, which shows 17, 15 and 50 nm for PMA^n, Fe_3O_4 and Fe_3O_4@silica/PIPA/PMA^n respectively, and their shapes are nearly spherical.

To investigate the size distribution of these nanoparticles, particle size histograms were prepared for Fe_3O_4, PMA^n, Fe_3O_4@silica and Fe_3O_4@silica/PIPA/PMA^n (Fig. 5a–d respectively) by DLS analysis. This size distribution is centered at a value of 12, 15, 35 and 45 nm for Fe_3O_4, PMA^n, Fe_3O_4@silica and Fe_3O_4@silica/PIPA/PMA^n respectively. Fig. 4e show SEM images of Fe_3O_4@silica/PIPA/PMA^n. As it is shown, these nanoparticles have spherical shapes with approximately 55 nm diameters.

In vitro release of PMA^n from the nano porous Fe_3O_4@silica/PIPA/PMA^n carrier was investigated. The drug loading and drug release content were measured from UV absorbance spectra on the basis of Beer–Lambert law:

$$A = \varepsilon c b$$

where, A is the absorption intensity, c is the PMA^n concentration, b is the path length of the radiation through the absorbing medium and ε is a proportionality constant. UV absorbance spectra of PMA^n and Fe_3O_4@silica/PIPA/PMA^n are shown in Fig. 2Ca and b respectively. By using UV data, PMA^n exhibit absorptions at λ_{max} = 350 nm [42].

The release profiles of PMA^n from Fe_3O_4@silica/PIPA/PMA^n for sample 1–4 are shown in Fig. 6a and b. As it is shown, with increases in loading content of drug in Fe_3O_4@silica/PIPA/PMA^n the release rate and the extent of released drug are increased. This may be due to the fact that the PMA is more soluble in the water than in PIPA and with the increase of the ratio of PIPA to PMA, the content of the free water in the hydrogels decreased.

According to Noyes–Whitney equation the dissolution rate is related to surface area:

$$\frac{dC}{dt} = kA(C_s - C)$$

where dC/dt, k, A, C_s and C are dissolution rate, dissolution rate constant, saturation solubility of the drug and concentration of drug in the bulk solution respectively. By decreasing the size of drug to nanometer range the total surface area is increased; therefore the

rate of dissolution and the rate of release are increased. As it is shown in Fig. 6b PMA^b has the slower release rate than PMA^n.

The release behavior of PMA^n from Fe_3O_4@silica/PIPA/PMA^n in different temperature or strength of magnetic field was investigated and the results are presented in Fig. 6c and d. It is well known that the solubility of PIPA in aqueous solution reduces with increasing temperature [6]. PIPA has been reported to have a lower critical solution temperature which is near 32 °C in water, based on viscosity, light scattering, and DSC studies [5]. As it is shown, PMA^n was released much faster by increasing the temperature from 35 to 55 °C (Fig. 6a), or increasing the strength of magnetic field from 500 to 570 G (Fig. 6b). This can be explained by the fact that the solubility is decreased due to a weakening of the ordering effect of the water–amide hydrogen bonds between the polymers as the temperature increases [20]. The data from Fig. 6c and d suggest that the PIPA gel in the Fe_3O_4@silica pores swells below the LCST (32 °C), and thus the PMA^n in the silica–PIPA gel cannot easily permeate through the pore. Above the LCST (32 °C) the PIPA gel shrinks so that PMA^n can easily be released through the pore.

4. Conclusions

For a drug to be absorbed, it must first be dissolved. By reducing the particle size to nanometer range, the total surface area, the rate of dissolution and the therapeutic response of a drug would increase. In this work, a new method is introduced for synthesis of nano drug; the particle size of $H_3PMo_{12}O_{40}$ is reduced to 15 nm by solvothermal method for the first time.

Fe_3O_4@SiO_2/poly(*N*-isopropylacrylamide) is synthesized as a novel magnetothermally responsive carrier for $H_3PMo_{12}O_{40}$ nano drug and characterized by TEM, SEM, DLS, FT-IR and XRD. Then the released behavior of $H_3PMo_{12}O_{40}$ nano-drug from this thermo-responsive carrier in an AC magnetic field was investigated. The rate of drug release is governed by:

1. The particle size of drug.
2. The strength of magnetic field.
3. The temperature of release medium.
4. The content of loaded drug.

By increasing the temperature from 35 to 55 °C, PMA^n was released much faster because above the LCST (32 °C) the PIPA gel shrinks so that PMA^n can easily be released through the pore. By increases in loading content of drug in the carrier the release rate and the extent of released drug are increased.

Acknowledgement

Authors are grateful to the council of Iran National Science Foundation and University of Kashan and Shiraz for their unending effort to provide financial support to undertake this work.

References

[1] M.N. Timofeeva, Appl. Catal. A-Gen. 256 (2003) 19.
[2] T. Yamase, Chem. Rev. 98 (1998) 307.
[3] D.E. Katsoulis, Chem. Rev. 98 (1998) 359.
[4] J.T. Rhule, C.L. Hill, D.A. Judd, Chem. Rev. 98 (1998) 327.
[5] S. Shigeta, S. Mori, T. Yamase, N. Yamamoto, N. Yamamoto, Biomed. Pharmacother. 60 (2006) 211.
[6] B. Hasenknopf, Front. Biosci. 10 (2005) 275.
[7] H.U.V. Gerth, A. Rompel, B. Krebs, J. Boos, C. Lanvers-Kaminsky, Anti-cancer Drugs 16 (2005) 101.
[8] A. Flütsch, T. Schroeder, M.G. Grütter, G.R. Patzke, Bioorg. Med. Chem. Lett. 21 (2011) 1162.
[9] D. Menon, R.T. Thomas, S. Narayanan, S. Maya, R. Jayakumar, F. Hussain, V.K. Lakshmanan, S.V. Nair, Carbohydr. Polym. 84 (2011) 887.
[10] F. Zhai, D. Li, C. Zhang, X. Wang, R. Li, Eur. J. Med. Chem. 43 (2008) 1911.
[11] C.S. Brazel, Pharm. Res. 26 (2009) 644.
[12] S. Laurent, S. Dutz, U.O. Häfeli, M. Mahmoudi, Adv. Colloid Interface 166 (2011) 8.
[13] R.E. Rosensweig, J. Magn. Magn. Mater. 252 (2002) 370.
[14] D.H. Kim, D.E. Nikles, D.T. Johnson, C.S. Brazel, J. Magn. Magn. Mater. 320 (2008) 2390.
[15] M. Prabaharan, J.F. Mano, Macromol. Biosci. 6 (2006) 991.
[16] T. Isojima, M. Lattuada, J.V.B. Sande, T.A. Hatton, ACS Nano 2 (2008) 1799.
[17] S.C. Jung, S.Y. Oh, Y.C. Bae, Polymer 50 (2009) 3370.
[18] C. Hofmann, M. Schönhoff, Colloid Polym. Sci. 287 (2009) 1369.
[19] J. Zhou, G. Wang, L. Zou, L. Tang, M. Marquez, Z. Hu, Biomacromolecules 9 (2008) 142.
[20] J. Lutz, O. Akdemir, A. Hoth, JACS 128 (2006) 13046.
[21] T. Kidchob, S. Kimura, Y. Imanishi, J. Chem. Soc. Perkin Trans. 2 (1997) 2195.
[22] G.H. Hsiue, S.H. Hsu, C.C. Yang, S.H. Lee, I.K. Yang, Biomaterials 23 (2002) 457.
[23] G. Huang, J. Gao, Z.B. Hu, J.V.S. John, B.C. Ponder, D. Moro, J. Control. Release 94 (2004) 303.
[24] Y. Qiu, K. Park, Adv. Drug Deliv. Rev. 53 (2001) 321.
[25] Z. Shen, W. Wei, Y.J. Zhao, G.H. Ma, T. Dobashi, Y. Maki, Z.G. Su, J.P. Wan, Eur. J. Pharm. Sci. 35 (2008) 271.
[26] K. Suzuki, T. Yumura, Y. Tanaka, M. Akashi, J. Control. Release 75 (2001) 183.
[27] D.J. Gan, L.A. Lyon, Macromolecules 35 (2002) 9634.
[28] X.J. Ju, S.B. Zhang, M.Y. Zhou, R. Xie, L. Yang, L.Y. Chu, J. Hazard. Mater. 167 (2009) 114.
[29] X.L. Zhao, X.B. Ding, Z.H. Deng, Z.H. Zheng, Y.X. Peng, X.P. Long, Macromol. Rapid Commun. 26 (2005) 1784.
[30] D. Schmaljohann, J. Oswald, B. Jorgensen, M. Nitschke, D. Beyerlein, C. Werner, Biomacromolecules 4 (2003) 1733.
[31] V. Polshettiwar, R. Luque, A. Fihri, H. Zhu, M. Bouhrara, J.M. Basset, Chem. Rev. 111 (2011) 3036.
[32] A. Schatz, O. Reiser, W.J. Stark, Chem. Eur. J. 16 (2010) 8950.
[33] A. Schatz, M. Hager, O. Reiser, Adv. Funct. Mater. 19 (2009) 2109.
[34] J. Meng, Ch. Shi, B. Wei, W. Yu, Ch. Deng, X. Zhang, J. Chromatogr. A 1218 (2011) 2841.
[35] Y.L. Yu, M.J. Zhang, R. Xie, X.J. Ju, J.Y. Wang, S.W. Pi, L.Y. Chu, J. Colloid Interface Sci. 376 (2012) 97.
[36] W. Zhao, J. Gu, L. Zhang, H. Chen, J. Shi, J. Am. Chem. Soc. 127 (2005) 8916.
[37] T. Uma, M. Nogami, Chem. Mater. 19 (2007) 3604.
[38] K.T. Venkateswara Rao, P.S.N. Rao, P. Nagaraju, P.S. Sai Prasad, N. Lingaiah, J. Mol. Catal. A-Chem. 303 (2009) 84.
[39] G.R. Rao, T. Rajkumar, B. Varghese, Solid State Sci. 11 (2009) 36.
[40] T.M. Quynh, M. Yoneyamab, Y. Maki, T. Dobashi, J. Appl. Polym. Sci. 123 (2012) 2368.
[41] M.K. Jaiswala, R. Banerjeeb, P. Pradhanb, D. Bahadura, J. Colloid Surf. B 81 (2010) 185.
[42] H.G. Manyar, G.S. Chaure, A. Kumar, J. Mol. Catal. A-Chem. 243 (2006) 244.
[43] H. Iida, K. Takayanagi, T. Nakanishi, T. Osaka, J. Colloid Interface Sci. 314 (2007) 274.
[44] M. Salavati-Niasari, J. Javidi, F. Davar, Ultrason. Sonochem. 17 (2010) 870.